NASA TN D-1380

TECHNICAL NOTE

D-1380

EFFECTS OF ANGLE OF ATTACK AND THICKNESS RATIO ON THE FLUTTER OF A RIGID UNSWEPT DIAMOND-AIRFOIL-SECTION WING AT A MACH NUMBER OF 10.0

By Lou S. Young

Langley Research Center
Langley Station, Hampton, Va.

NATIONAL AERONAUTICS AND SPACE ADMINISTRATION
WASHINGTON August 1962

NATIONAL AERONAUTICS AND SPACE ADMINISTRATION

TECHNICAL NOTE D-1380

EFFECTS OF ANGLE OF ATTACK AND THICKNESS RATIO ON THE FLUTTER OF A RIGID UNSWEPT DIAMOND-AIRFOIL-SECTION WING AT A MACH NUMBER OF 10.0

By Lou S. Young

SUMMARY

A flutter investigation at a Mach number of 10.0 has been made of two unswept untapered diamond-airfoil-section wings in the Langley 15-inch hypersonic-flow apparatus. The wings had airfoil sections with thickness ratios of 0.11 and 0.15 and were each tested at angles of attack up to 10°. The models had rigid-body degrees of freedom in pitch about the center line and in translation normal to the plane of the wing. The wing had sufficient stiffness that the vibration modes involving the wing had considerably higher frequencies than the two rigid-body modes. The results were compared with third-order piston-theory calculations.

Increasing the thickness ratio decreased the flutter velocity parameter, and increasing the angle of attack also decreased the flutter velocity parameter at least at angles of attack up to 10°. The calculated flutter velocity parameters are in fair agreement with experiment. The agreement was somewhat better for the 15-percent-thick wing than for the 11-percent-thick wing. The calculated flutter frequencies were much higher than the experimental frequencies.

INTRODUCTION

Piston theory has been applied extensively to the analysis of aeroelastic problems in the supersonic and hypersonic speed regimes. (See, for example, refs. 1 and 2.) Its application to higher and higher Mach numbers is questionable, however, because of a basic assumption in the derivation of the theory which states that the downwash velocity at the airfoil surface must not exceed the speed of sound. Stated another way, the product of Mach number and local slope of the airfoil surface must not exceed one. For many combinations of Mach number and airfoil shape this limitation of the theory is not a serious restriction, but for thick airfoils at high Mach numbers and especially at appreciable angles of attack, the product of Mach number and local surface slope can be considerably greater than one.

Since both theory and experiment indicate an unfavorable effect on the flutter characteristics of increasing airfoil thickness and the theory indicates an unfavorable effect of angle of attack, the influence of these variables on aeroelastic characteristics may be quite important, as pointed out in reference 3. In order to obtain an evaluation of some effects of thickness and angle of attack and a further indication of the range of applicability of piston theory, a flutter investigation was made on simple rigid spring-mounted models at a Mach number of 10 in the Langley 15-inch hypersonic-flow apparatus. Airfoils having thickness ratios of 0.11 and 0.15 were tested at angles of attack up to 10°. The experimental results are compared with results obtained from piston-theory flutter calculations.

SYMBOLS

b	semichord, ft
K_h	spring stiffness in translation, lb/ft
K_θ	spring stiffness in pitch, ft-lb/radian
m_h	"effective" mass of model in translation, slugs
m_θ	effective mass of model in pitch, slugs
M	Mach number
q	free-stream dynamic pressure, lb/sq ft
r_θ	nondimensional effective radius of gyration of model about the pitch axis, $\frac{\text{Effective radius of gyration}}{b}$
s	span of airfoil, ft
T_t	stagnation temperature, $^{\circ}R$
V	free-stream velocity, ft/sec
x_o	nondimensional distance from airfoil leading edge to pitch axis, $\frac{\text{Distance from leading edge to pitch axis}}{2b}$

$x_{cg,\theta}$ nondimensional effective center-of-gravity location with respect to pitch axis, positive when center of gravity is behind pitch axis, $\frac{\text{Distance from pitch axis to effective center of gravity}}{b}$

β angle between translation direction and normal-force direction, deg

γ ratio of specific heats (taken to be 1.4)

θ model pitch angle or angle of attack, deg or radians

λ ratio of effective pitching mass to effective translating mass, m_θ/m_h

μ_h mass ratio based on translating mass, $\frac{m_h}{4s\rho b^2}$

ξ half-angle of diamond-airfoil section, deg

ρ free-stream static density, slug/cu ft

t/c thickness ratio of airfoil section

ω flutter frequency, radians/sec

ω_h frequency of uncoupled translation vibration mode, radians/sec

ω_θ frequency of uncoupled pitch vibration mode, radians/sec

ω_c frequency of coupled pitch vibration mode, radians/sec

ω_b frequency of lowest mode involving airfoil and mount flexibilities, radians/sec

Ω square of frequency ratio, $\left(\omega_h/\omega_\theta\right)^2$

MODELS

Design and Construction

A moderately high-aspect-ratio, unswept, untapered planform was chosen so that the air forces would be two dimensional over almost all

the span. The planform, shown in figure 1(a), was the same for the two wings (t/c = 0.11 and 0.15). Some geometrical properties of the wings are listed in table I. The wings were constructed of two pieces of cobalt-alloy material which were bent, welded together, and ground to size (fig. 1(a)). The Inconel shaft of each model supported the wings in the tunnel as shown in figure 1(b) and provided connection to the support mechanism (shown schematically in fig. 2), which allowed the rigid-body freedoms in pitch and translation. The materials and methods employed in the model construction were chosen for the following reasons: (1) to avoid melting or distortion of the airfoil resulting from aerodynamic heating, (2) to prevent heating of the support mechanism, (3) to keep the model mass within acceptable limits, and (4) to provide the wings and their supporting shafts with sufficient stiffness so that the natural vibration modes involving airfoil and support flexibilities had considerably higher frequencies than the rigid-body translation and pitching modes of the models.

The shaft and support mechanism were shielded from the airstream as shown in figures 1(b) and 3(a). The splitter plate and shaft shield (fig. 1(b)) were carefully constructed and alined with the airstream to avoid a shock wave off the splitter plate upstream of the wing. A slot in the splitter plate (fig. 1(b)) allowed clearance for the model shaft. A small shield affixed to the shaft (fig. 3(b)) reduced the airflow through the slot.

Two manually operated devices were used to prevent model motion during the tunnel starting and stopping transients, to stop flutter motion, and to agitate the model during testing. These devices are shown in the photograph in figure 3(b). One had four prongs which swung on the end of a spring so that it engaged the model frame and pitch-spring lever-arm, and the other was a cam-operated "duck-bill" which clamped the model shaft.

Physical Properties

The inertia properties of the models are listed in table I. It should be noted that the design of the support mechanism gave rise to the two mass terms m_h and m_θ because only part of the translating portion of the model could also move in pitch. The values given for m_θ, m_h, r_θ^2, and $x_{cg,\theta}$ are the "effective" values which were obtained from the measured inertia properties shown on the right-hand side of the following equations:

$$m_\theta = m_r + \frac{2}{3}m_p$$

$$m_h = m_r + 2m_p + m_f + 2\frac{I_A}{l_A^2} + \frac{2}{3}m_t$$

$$R_\theta^2 = \frac{I_r + \frac{2}{3}m_p l^2}{m_\theta b^2}$$

$$x_{cg,\theta} = \frac{m_r x_r + m_p l}{m_\theta b}$$

where

m_r mass of that portion of model which rotates about pitch axis

m_p mass of one pitch coil spring

m_f mass of frame

m_t mass of one translation coil spring

I_A mass moment of inertia of one translation arm about fixed pivot

I_r mass moment of inertia of mass m_r about pitch axis

l_A length of translation arm between pivots

l distance from pitch axis to pitch spring center line

x_r distance from pitch axis to center of gravity of m_r

The translation and pitching stiffnesses and the natural vibration frequencies are presented in table II along with the experimental data which are discussed subsequently. The translation stiffness was measured by means of a cathetometer before the model was mounted in the tunnel. The model could not be easily dismounted from the tunnel; therefore, the pitching stiffness was measured by means of an inclinometer mounted on the model. Measurements made with the inclinometer are probably less accurate than cathetometer measurements would be. The natural vibration frequencies were determined before each run by exciting the model by means of either an electromagnetic shaker or by plucking the model under a strobatac light. The two methods were found to give the same results. The values listed in table II in the

column ω_h, the uncoupled translation frequency, are actually the measured coupled translation frequencies. A measurement of the true uncoupled frequency (pitch freedom locked out) was made and it was found to be the same as the coupled translation frequency within the measurement accuracy. The uncoupled pitching frequency ω_θ (obtained by locking out the translation freedom) and the coupled pitching frequency ω_c are somewhat different (table II). The mode associated with the frequency ω_b in table II involved flexibilities of the model shaft and the support system. The mode shape appeared similar to a cantilever bending mode but included some pitching.

APPARATUS AND TESTS

The tests were made at $M = 10.0$ in the Langley 15-inch hypersonic-flow apparatus which is a blowdown facility having an axisymmetric contoured nozzle. The tests were made in air at stagnation temperatures between about $1,300^\circ$ F and $1,500^\circ$ F. Viewing ports 13 inches in diameter are provided on each side of a 15-inch-diameter test section. The present investigation was carried out at stagnation pressures between 576 and 1,500 pounds per square inch absolute, which represent Reynolds numbers based on chord between 1.7×10^5 and 5.4×10^5.

For the present tests the window in one of the viewing ports was replaced by a steel plate to which the model and the splitter plate were mounted (figs. 1(b) and 3) so that the wing was out of the tunnel-wall boundary layer. Figure 4 shows the layout of the tunnel with the model in place.

During a test run (defined as a single operation of the tunnel from upstream valve opening to valve closing), the model was clamped until the flow was established. The stagnation temperature was then brought up to the operating value. During this process, which required about 30 seconds, the wing reached equilibrium temperature. The stagnation pressure was then gradually increased until flutter was obtained. In most of the runs it was necessary to agitate the model with one of the clamping devices in order to initiate flutter because the tunnel airflow is very smooth. The model was clamped before the tunnel was shut down. Before the wing was to be tested at an angle of attack the steel plate which supported the model and the slot in the splitter plate were rotated to the desired angle. The splitter plate and shaft shield remained at zero angle of attack.

In order to test the wing at angles of attack, it was necessary to adjust the lengths of the pitch and translation springs so that the wing

deflections under steady-state air loads would place it near the center of the tunnel at the desired angle of attack when the flutter stagnation pressure was reached. If the angle of attack presetting was too large or too small, the angle between the normal force and the translation direction β would be a negative or a positive value, respectively. The model angle at flutter was in most cases different from the intended angle because the flutter stagnation pressure was unknown prior to each run.

During one of the test runs with the wing at zero angle of attack, observations were made on an oil film on the wing and splitter plate in order to detect the presence of shock waves which would indicate misalinement of the splitter plate in the flow. No significant shock waves were observed.

The model was instrumented for the tests by means of electromagnetic pickups mounted above and below the model (fig. 3(b)) which fed indications of the model translation oscillations to a recording oscillograph. The oscillograph records were used to identify the start of flutter and to obtain the flutter frequency. A motion-picture camera was employed to provide a record of the angle of attack. Tunnel stagnation pressure and temperature were continuously recorded on pen-type recorders. Reference signals were provided so that the oscillograph records, motion pictures, and tunnel conditions could be correlated. Because of the nonlinearity of the output of the electromagnetic pickups with model position, it was not possible to determine a decrement-of-motion record for the purpose of determining the amount of friction in the apparatus with reasonable accuracy.

ANALYSIS

The two-degree-of-freedom, uncoupled-mode analysis employed rigid-body modes in pitch about the wing midchord and in translation normal to the plane of the wing. The air forces were obtained from third-order piston theory for a diamond-airfoil section as in reference 4. It should be noted that the derivation of the piston-theory air forces is based on the condition that the hypersonic similarity parameter $M\frac{t}{c}$ be much smaller than unity.

The method of analysis allowed a closed-form solution of the flutter determinant (with the friction or damping of the model support taken as zero):

$$\frac{V}{b\omega_\theta\sqrt{\mu_h}} = \sqrt{\frac{M\lambda}{C}\left[\frac{\lambda\left(x_{cg,\theta}\right)^2D^2 + r_\theta^2(D - C)(\Omega C - D)}{S_2\Omega C + DE}\right]}$$

and

$$\omega = \omega_\theta \sqrt{\frac{D}{C}}$$

where

$$C = \lambda\left(r_\theta^2 S_1 - 2x_{cg,\theta} S_2\right) + S_3$$

$$D = \lambda r_\theta^2 S_1 + S_3 \Omega$$

$$E = \left(\frac{S_2^2 - S_1 S_3}{M\mu_h}\right) + \lambda x_{cg,\theta} S_1 - S_2$$

$$S_1 = F$$

$$S_2 = -G + F(1 - 2x_o)$$

$$S_3 = (1 - 2x_o)\left[-2G + F(1 - 2x_o)\right] + \frac{F}{3}$$

$$F = 1 + \frac{\gamma + 1}{4} M^2 \left[\theta^2 + (t/c)^2\right]$$

$$G = \frac{\gamma + 1}{4} M \frac{t}{c}$$

As was noted previously, the translating and pitching portions of the model had different masses (m_h and m_θ, respectively). In the analysis a mass ratio μ_h was defined only for m_h, and m_θ appears only in the form of λ, which is the ratio of m_θ to m_h.

Although the term in parentheses in the equation for E contains the mass ratio μ_h, for the present investigation the product $M\mu_h$ was

so high that this term was negligible in comparison to the other terms. The solution was modified to include the effect of the angle between the translation and normal-force directions β but calculations made for values of β up to 4° showed negligible differences due to this angle.

It should be noted that for the 11-percent-thick diamond-airfoil section, the value of $M\frac{t}{c}$ is about unity at $\theta = 0^{\circ}$, which is marginal for piston-theory applicability. The 15-percent-thick diamond-airfoil section was chosen both to obtain experimental data and to evaluate piston-theory predictions at an even higher value of $M\frac{t}{c}$. The values of x_o and $x_{cg,\theta}$ were chosen so that the models would be sensitive flutter cases.

Reference 3 describes a method of obtaining oscillatory air forces for high values of $M\frac{t}{c}$, wherein aerodynamics obtained from a combination of piston theory and shock-expansion theory are used. The steady-state pressures obtained from shock-expansion theory are employed to account for the effects of thickness and angle of attack, and the unsteady pressure contributions of the normal translation and pitch modes are obtained from first-order piston theory. Calculations made for the present data by this method showed no significant differences from the third-order piston-theory calculations, as in reference 3.

RESULTS AND DISCUSSION

The experimental results of the investigation are presented in table II and are plotted in figures 5 and 6 along with the analytical results.

As was mentioned previously, in order to initiate flutter the model normally had to be agitated by means of one of the locking devices. All the start-of-flutter points obtained on the 11-percent-thick wing except in run 3 (table II) were obtained just after the model was agitated or while the model was still oscillating after being agitated. The model had been agitated prior to flutter in run 3, but was motionless just before the start of flutter. Without agitation, the model generally would not flutter, as illustrated in table II by run 1. At point 1 of run 1 the model without agitation was flutter free at a dynamic pressure about 7 percent higher than that of point 2, which is the flutter point obtained with agitation.

11-Percent-Thick Wing

The flutter mode for the 11-percent-thick wing appeared to consist of translation and very small pitching oscillations, wherein the leading edge pitched up as the model translated down, and the motions reached maximum amplitude with the same sign at about the same time. As can be seen in table II, the flutter frequency is quite close to the uncoupled translation frequency ω_h. Except for run 5, the flutter was characterized by a very gradual increase in amplitude either after an abrupt start or after a decrease in the amplitude of the oscillations produced by agitating the model. The amplitude tended to reach a constant value, only increasing or decreasing as the pressure was raised or lowered. The flutter obtained in run 5 was of the same type but was definitely divergent.

The experimental flutter points obtained on the 11-percent-thick wing (indicated by F in the column "Model behavior" in table II) are plotted in figure 5 for $\frac{V}{b\omega_\theta\sqrt{\mu_h}}$ as a function of angle of attack. The flutter speed decreased as the angle of attack was increased until a flutter speed about 11 percent below that obtained at $\theta = 0^\circ$ was obtained at $\theta = 7.9^\circ$. One flutter point and one no-flutter point were obtained at angles of attack above 7.9°, and these appear to indicate an abrupt increase in flutter speed to a value at $\theta = 10.2^\circ$ which is only about 3 percent below that obtained at $\theta = 0^\circ$. These data near $\theta = 10^\circ$ are believed to be incorrect because in the two runs (runs 4 and 5, table II) the aerodynamic heating caused a severe warp in the wing, amounting to about 1/2 inch at the tip. The warp may have caused the wing root to bind against the splitter plate (note that the flutter frequency of run 5 is higher than for the other flutter points in table II) or the changed pitch mode due to the warp may have raised the flutter speed. The wing was not discernibly warped in any of the other runs. It should be pointed out that the frequency ratio ω_h/ω_θ for these two runs was lower than for the other runs on this model. However, it is felt that this difference was not sufficiently large to cause the apparent reversal of trend of flutter speed with angle of attack. The calculated results indicated only a small effect of the frequency ratio differences.

As can be seen in figure 5, except for the experimental points near $\theta = 10^\circ$, the analytical results for the 11-percent-thick wing are lower than the experiment but agree to within 6 percent and appear to predict the trend of flutter speed with angle of attack. This agreement is surprising in view of the large value of $M\frac{t}{c}$ for this model. However, the calculated flutter frequencies show poor agreement with the experiment as can be seen in figure 6, which is a plot of ω against angle of attack. The calculated frequencies are as much as 64 percent higher than

the experimental frequencies. Furthermore, the calculations indicate an increasing trend of ω with θ, whereas the experiment (except for the point at $\theta = 10.2^{\circ}$) indicates the opposite trend. Since damping of the model-support system could not be measured, it is not possible to make a complete evaluation of the effects of damping on the comparison of calculated and measured results. A calculation for one test condition was made by using a reasonable value for damping ($g = 0.02$) and it was found that the agreement in flutter velocity was decreased from 5 percent to 12 percent, while the agreement in flutter frequency increased from 30 percent to 3 percent.

15-Percent-Thick Wing

The 15-percent-thick wing also had to be agitated to initiate flutter, except in run 6 (table II). In run 6 the model had been agitated prior to flutter but was motionless just before the start of flutter. The flutter mode for the 15-percent-thick wing was similar to that of the 11-percent-thick wing. Except for run 7, the amplitude of flutter increased slowly after the start, in the same manner as the thinner wing. In run 7 the flutter amplitude diverged rapidly.

The experimental results for the 15-percent-thick wing, which are plotted in figure 5, also indicate a decrease in flutter speed as angle of attack is increased. The flutter speed at $\theta = 9.7^{\circ}$ is about 12 percent below that obtained at $\theta = 0^{\circ}$.

The analytical results for the 15-percent-thick wing (fig. 5) agree well with the experimental results. The trend of flutter speed with angle of attack is in fairly close agreement and the analytical and experimental results agree to within about 4 percent. The calculated flutter frequencies for this wing (fig. 6) are as much as 96 percent higher than the experimental frequencies, and for this wing, also, opposite frequency trends are indicated by experiment and theory.

Effect of Airfoil Thickness

As can be seen in tables I and II, ω_θ and μ_h are the only quantities among the physical properties and test conditions which are significantly different for the 11-percent- and 15-percent-thick wings. The differences in μ_h values are probably of small importance since this parameter is shown in the calculations to have little effect and the experimental data (table II) do not indicate a large mass-ratio effect. The parameter $\frac{V}{b\omega_\theta\sqrt{\mu_h}}$ has been shown to correlate flutter data for differences in ω_θ at Mach numbers into the low supersonic range.

Therefore, and in view of the small differences in ω_θ between the thicker and thinner airfoil sections, it may be assumed that the parameter $\frac{V}{b\omega_\theta\sqrt{\mu_h}}$ provides an adequate standard for a qualitative comparison at the two thickness ratios.

It can be seen in figure 5 that the increase in thickness ratio decreased the flutter velocity parameter. The analytical results predict a smaller effect of thickness than was obtained experimentally.

CONCLUSIONS

A flutter investigation has been made at a Mach number of 10.0 on two diamond-section-airfoil wings which had rigid-body pitching and translation degrees of freedom. Wings having airfoil thickness ratios of 0.11 and 0.15 were each tested at angles of attack up to about 10°. The results were compared with third-order piston-theory calculations. The following conclusions can be drawn for the conditions of this investigation:

1. Increasing thickness ratio decreases the flutter velocity parameter.

2. Increasing angle of attack decreases the flutter velocity parameter at least at angles of attack up to 10°.

3. The calculated flutter velocity parameters are in fair agreement with experiment and the agreement was somewhat better for the 15-percent-thick wing than for the 11-percent-thick wing. The calculated flutter frequencies were much higher in all cases than the experimental frequencies.

Langley Research Center,
National Aeronautics and Space Administration,
Langley Station, Hampton, Va., May 18, 1962.

REFERENCES

1. Morgan, Homer G., and Miller, Robert W.: Flutter Tests of Some Simple Models at a Mach Number of 7.2 in Helium Flow. NASA MEMO 4-8-59L, 1959.

2. Hanson, Perry W.: Aerodynamic Effects of Some Configuration Variables on the Aeroelastic Characteristics of Lifting Surfaces at Mach Numbers From 0.7 to 6.86. NASA TN D-984, 1961.

3. Morgan, Homer G., Runyan, Harry L., and Huckel, Vera: Theoretical Considerations of Flutter at High Mach Numbers. Jour. Aero. Sci., vol. 25, no. 6, June 1958, pp. 371-381.

4. Zartarian, Garabed, Heller, Alfred, and Ashley, Holt: Application of Piston Theory to Certain Elementary Aeroelastic Problems. Proc. Fourth Midwestern Conf. on Fluid Mechanics, Res. Ser. No. 128, Purdue Eng. Exp. Station, 1955, pp. 163-181.

TABLE I.- MODEL GEOMETRICAL AND INERTIAL PROPERTIES

Property	11-percent-thick wing	15-percent-thick wing
s, ft	0.5817	0.5833
b, ft	0.1017	0.1042
Area, sq ft	0.1183	0.1216
Panel aspect ratio . .	2.86	2.84
Taper ratio	1.00	1.00
Airfoil section	Diamond	Diamond
t/c	0.1062	0.1505
ξ, deg	6.06	8.56
x_o	0.5000	0.5000
m_h, slug	0.01885	0.01900
m_θ, slug	0.01219	0.01234
λ	0.6468	0.6496
r_θ^2	0.5289	0.5036
$x_{cg,\theta}$	0.2378	0.2321

TABLE II.- EXPERIMENTAL RESULTS

Wing	Run	Point	Model behavior (a)	K_h, lb/ft	K_θ, $\frac{\text{ft-lb}}{\text{radian}}$	ω_h, $\frac{\text{radian}}{\text{sec}}$	ω_θ, $\frac{\text{radian}}{\text{sec}}$	ω_c, $\frac{\text{radian}}{\text{sec}}$	ω_b, $\frac{\text{radian}}{\text{sec}}$	ω_h/ω_θ	θ, deg	β, deg	q, $\frac{\text{lb}}{\text{sq ft}}$	T_t, $^\circ R$	ρ, $\frac{\text{slug}}{\text{cu ft}}$	V, ft/sec	ω, $\frac{\text{radian}}{\text{sec}}$	μ_h	$\frac{V}{b\omega_\theta\sqrt{\mu_h}}$	Remarks
11 percent thick	1	1	Q	66.9	1.29	59.1	148.9	151.4	226.2	0.3966	0	0	197.0	1,855	1.855×10^{-5}	4,608	----	----------	-----	Model was not agitated
	1	2	F		1.29	59.1	148.9	151.4	226.2	.3966	0	0	184.3	1,820	1.769	4,565	71.0	4.427×10^{4}	1.433	Model was agitated as q was increased again
	2	1	F		1.29	60.2	152.1	155.2	223.7	.3959	4.1	1.6	172.8	1,845	1.637	4,595	69.1	4.784	1.359	
	3	1	F		1.29	59.1	151.4	152.1	226.2	.3900	7.9	2.9	150.5	1,820	1.445	4,564	67.2	5.420	1.273	Flutter obtained without agitation
	4	1	Q		1.78	60.0	169.6	170.3	219.9	.3537	≈10	≈0	219.1	1,860	2.058	4,614	----	3.805	1.371	θ only approximate (motion-picture film ran out)
	5	1	F		1.78	59.1	169.0	169.6	211.7	.3499	10.2	-1.8	217.7	1,843	2.064	4,593	90.6	3.794	1.384	Divergent flutter followed by violent irregular oscillations; model damaged
15 percent thick	6	1	F	66.9	1.82	59.6	182.2	179.7	288.4	0.3270	0	0	181.8	2,016	1.575×10^{-5}	4,803	67.9	4.761×10^{4}	1.159	Flutter obtained without agitation
	7	1	F		1.82	59.1	179.1	179.7	289.0	.3298	6.6	1.6	172.0	1,891	1.589	4,653	68.5	4.719	1.148	Divergent flutter
	7	2	F		1.82	59.1	179.1	179.7	289.0	.3298	5.9	.9	170.6	1,910	1.560	4,676	68.5	4.807	1.143	Divergent flutter
	8	1	F		1.82	59.6	179.1	182.2	281.5	.3326	9.7	-.2	135.1	1,858	1.270	4,612	64.7	5.904	1.017	

[a] F stands for flutter; Q stands for maximum pressure reached without obtaining flutter.

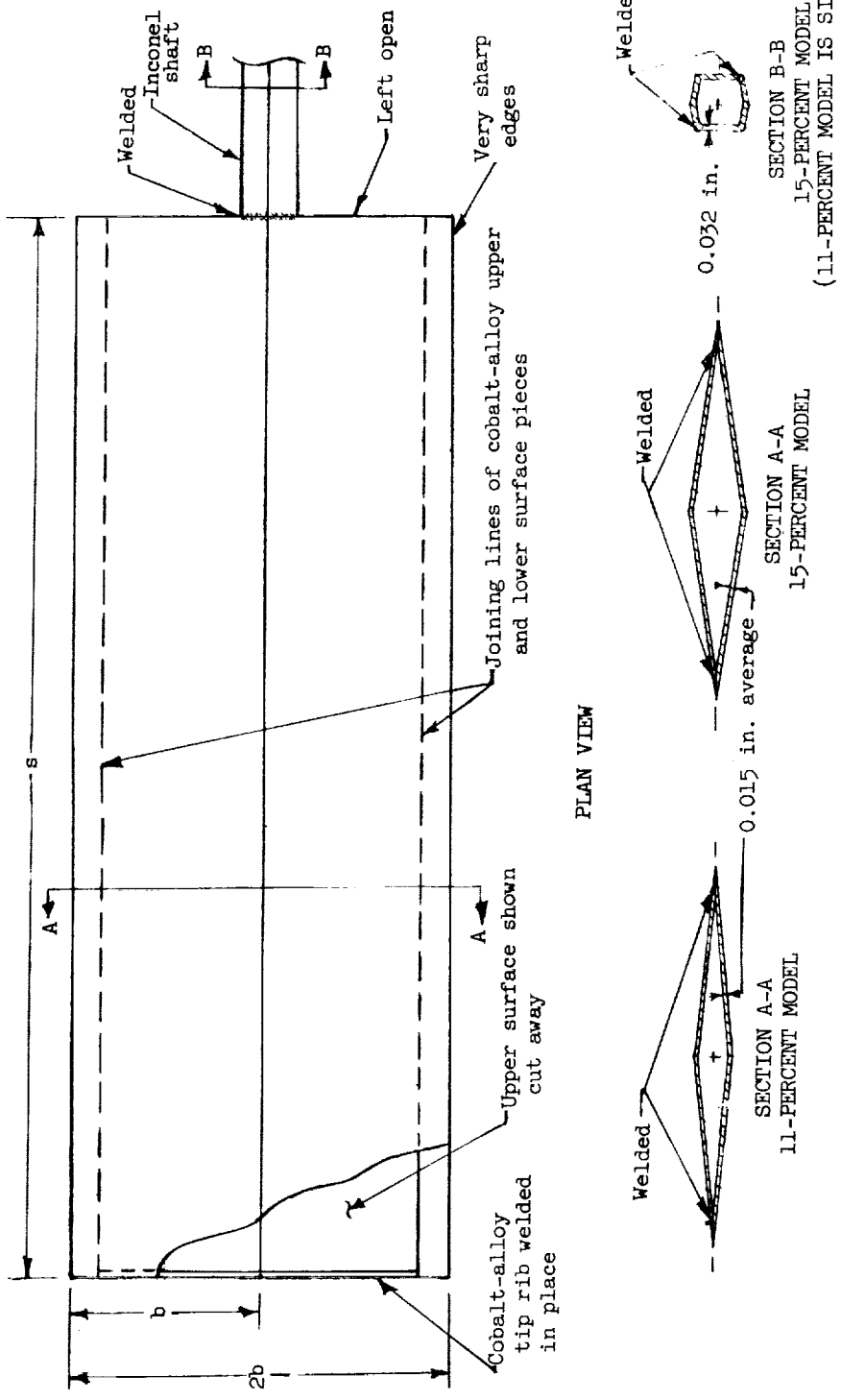

(a) Details of the airfoils.

Figure 1.- Sketch of the model.

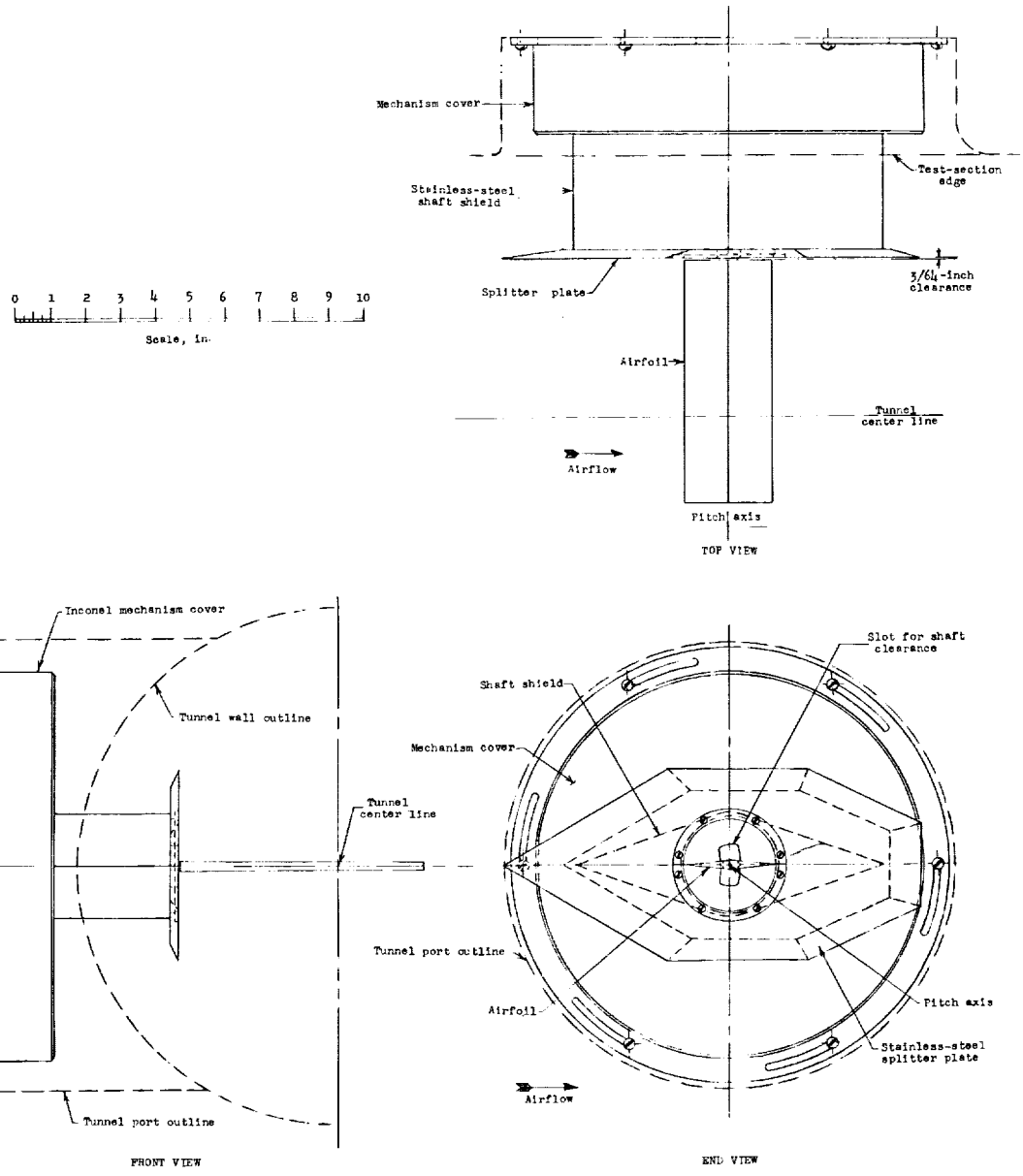

(b) External details of model.

Figure 1.- Concluded.

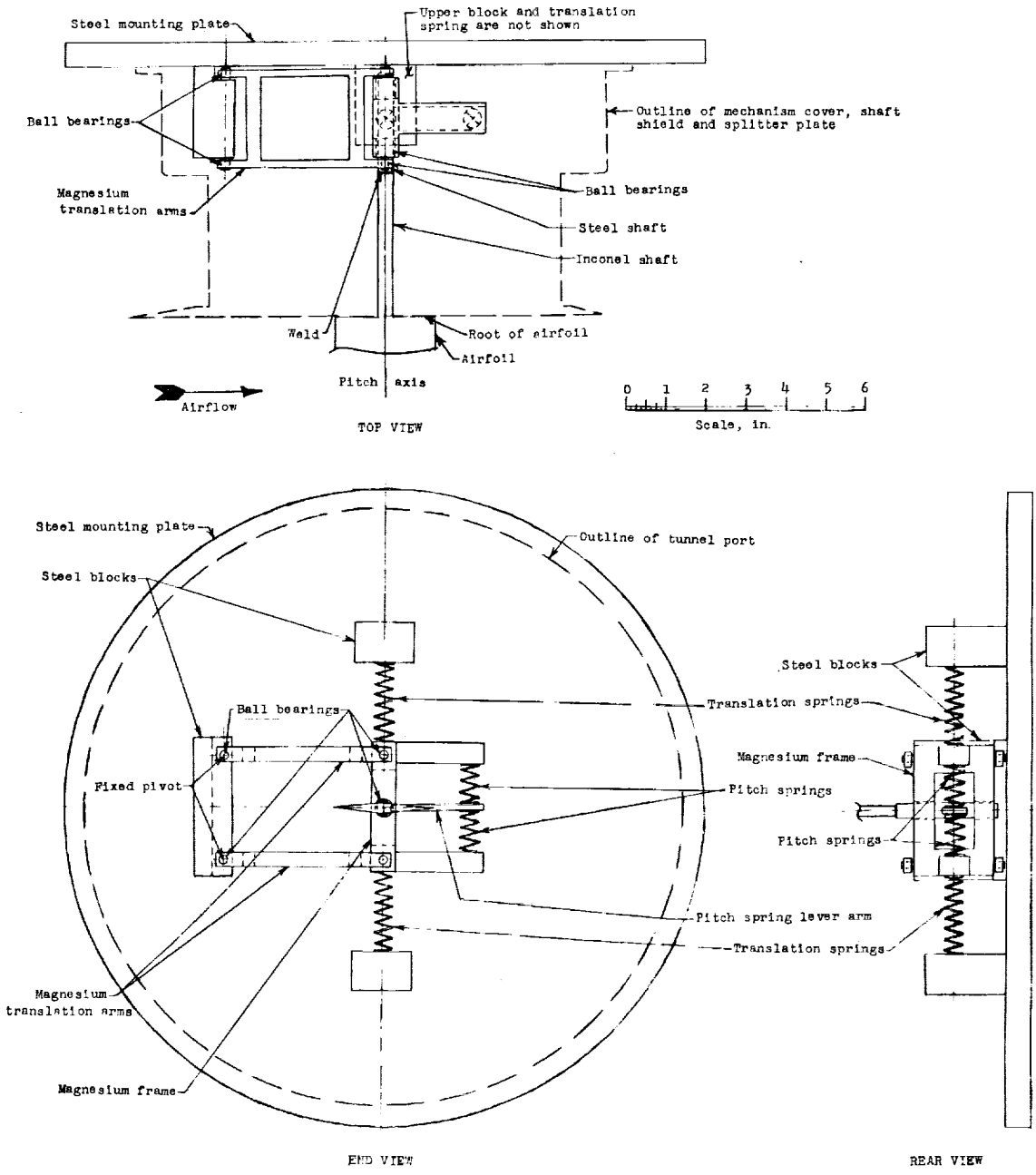

Figure 2.- Schematic sketch of model support mechanism.

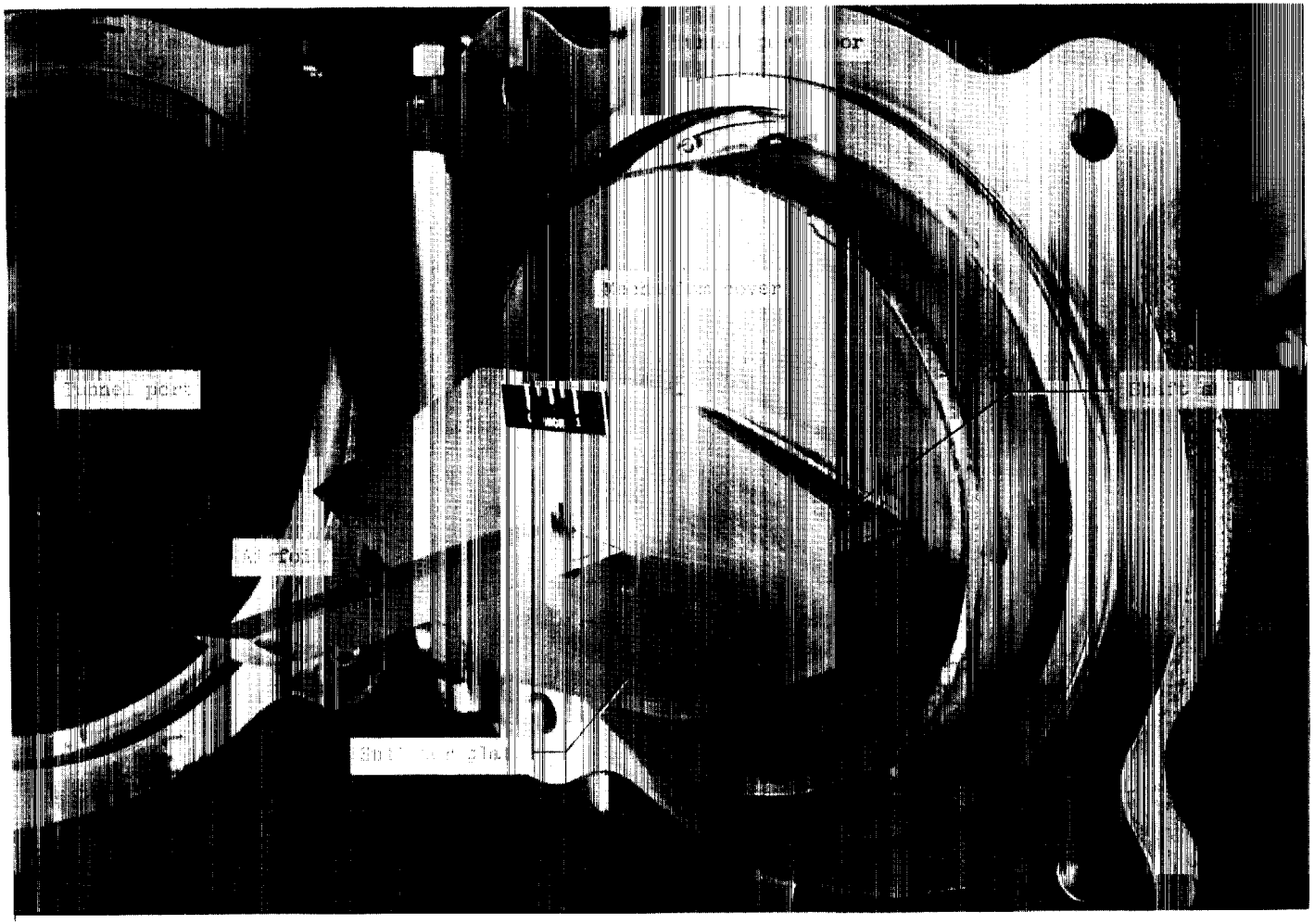

(a) Model at 0° angle of attack. L-60-1903.1

Figure 3.- Photographs of model.

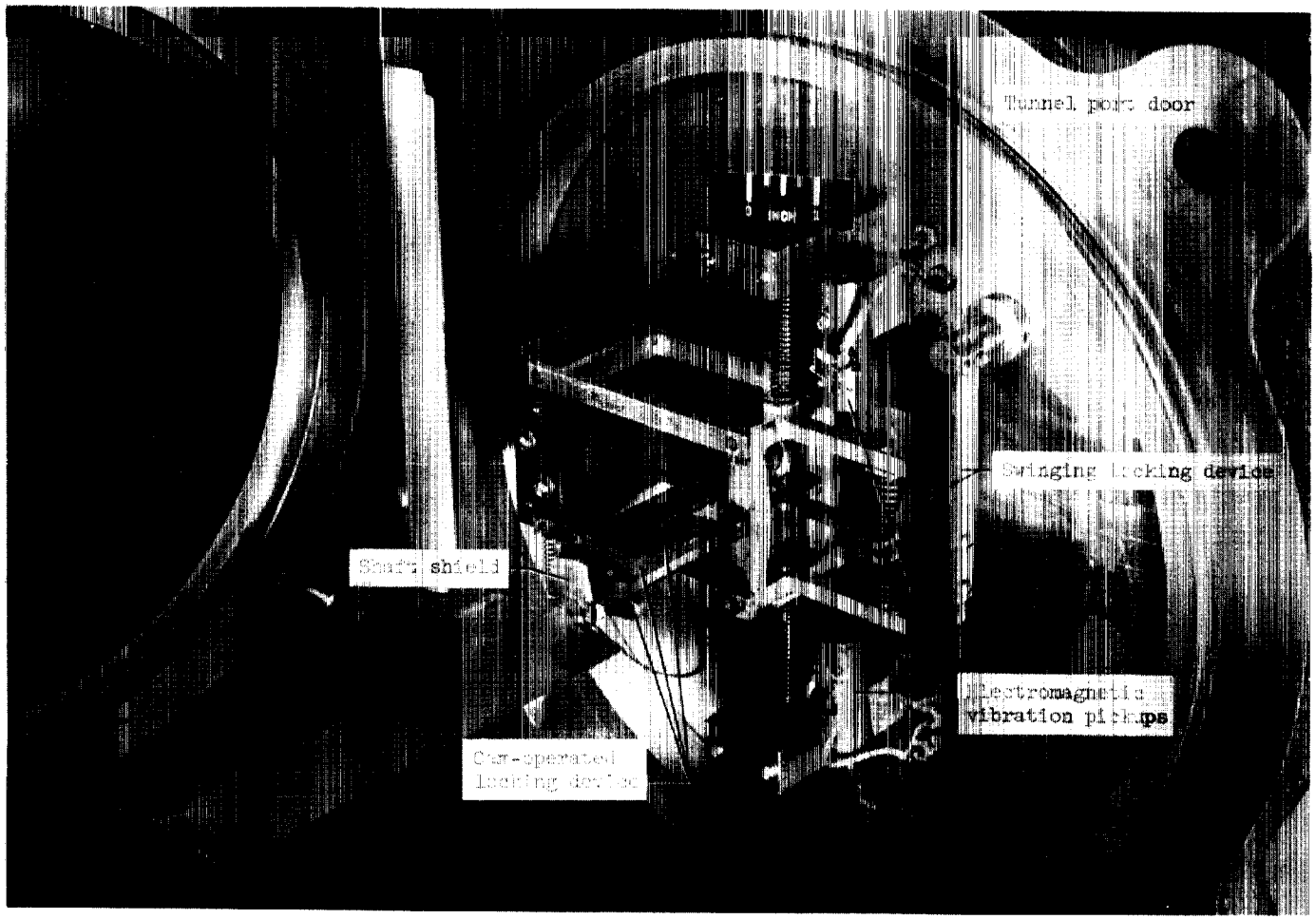

L-60-1900.1

(b) Support mechanism at 0° angle of attack; model locked. (Only parts not shown in fig. 2 are labeled.)

Figure 3.- Concluded.

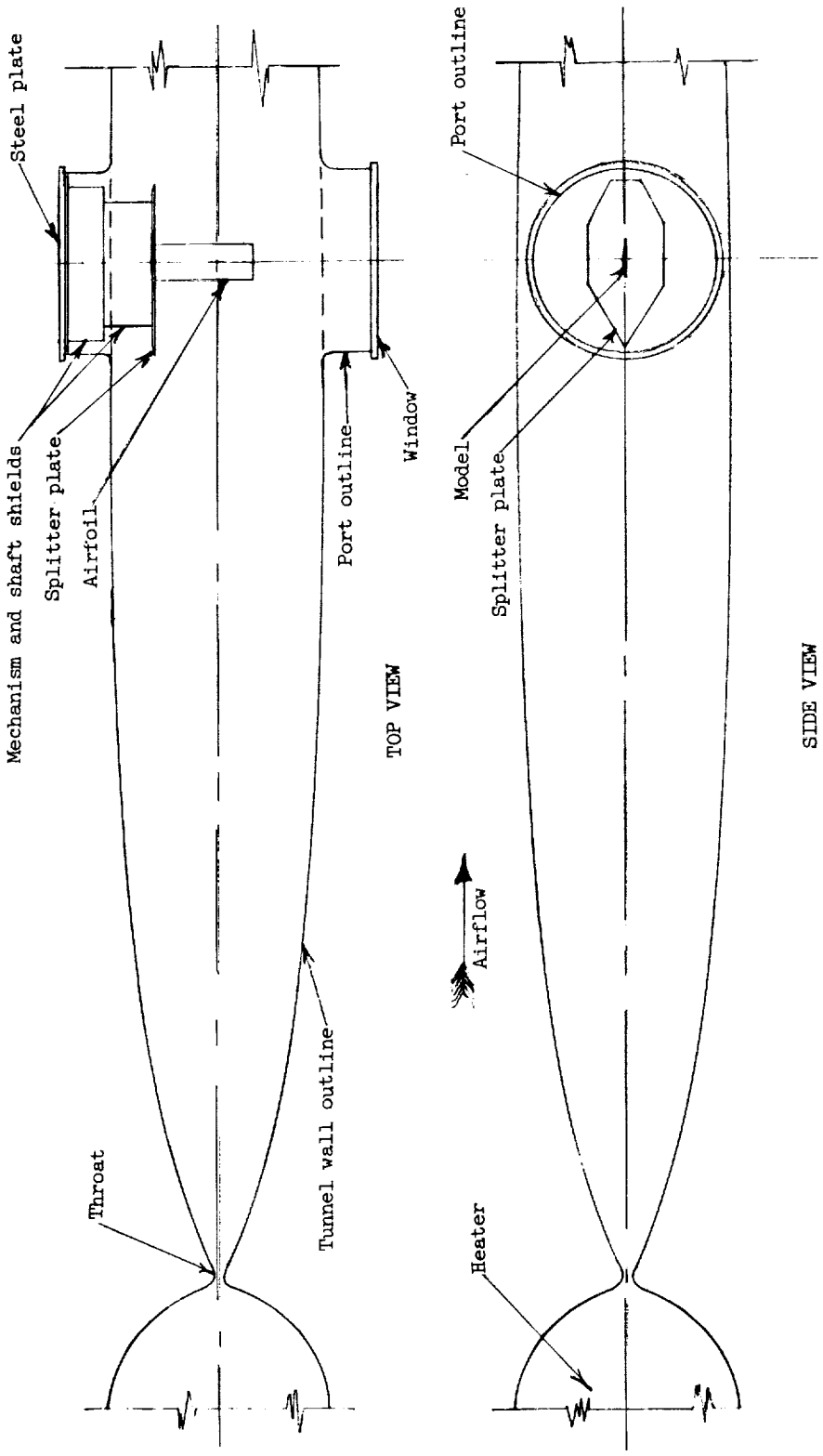

Figure 4.- Sketch of the model in the hypersonic-flow apparatus.

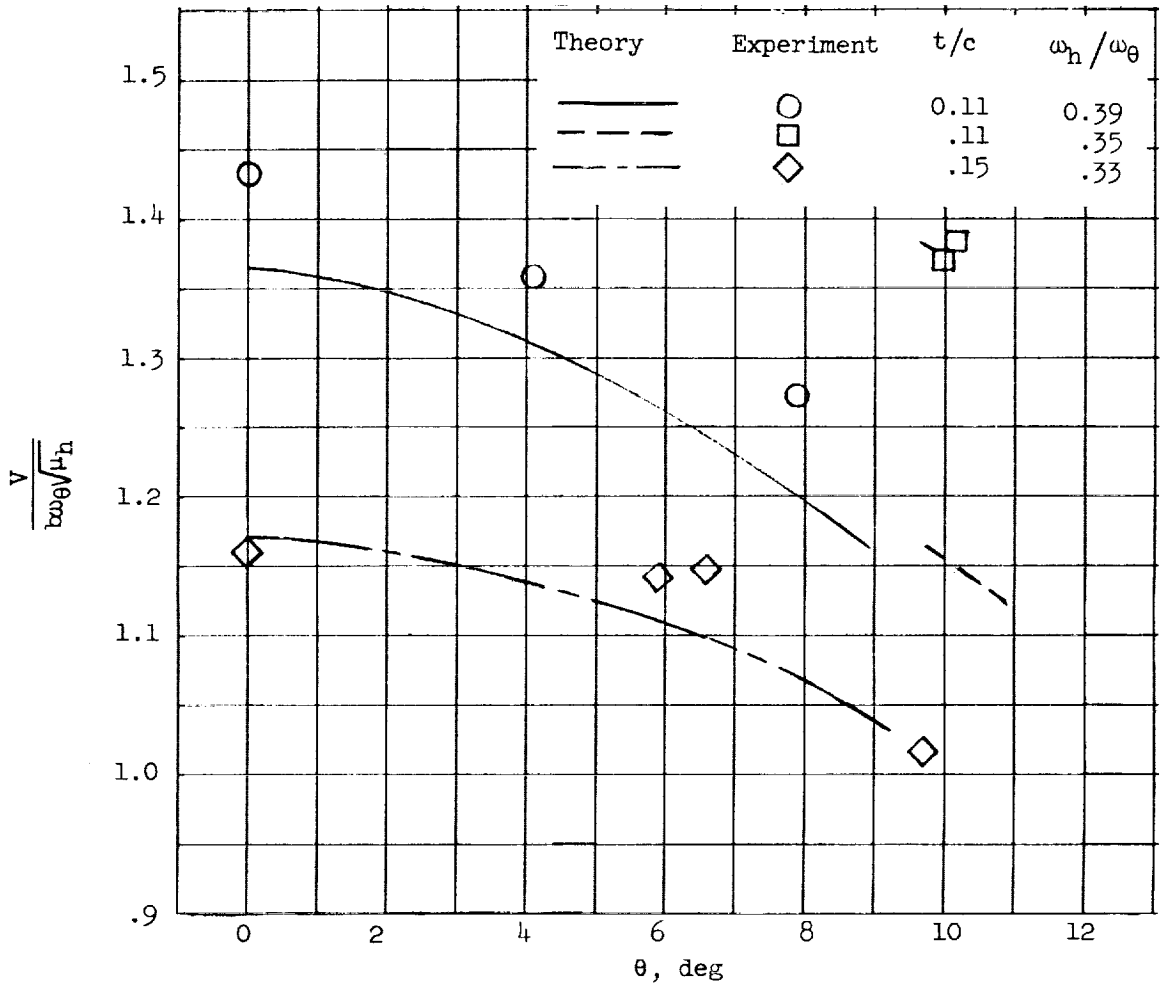

Figure 5.- Experimental and calculated results. Flagged symbol indicates a maximum dynamic pressure, no-flutter point.

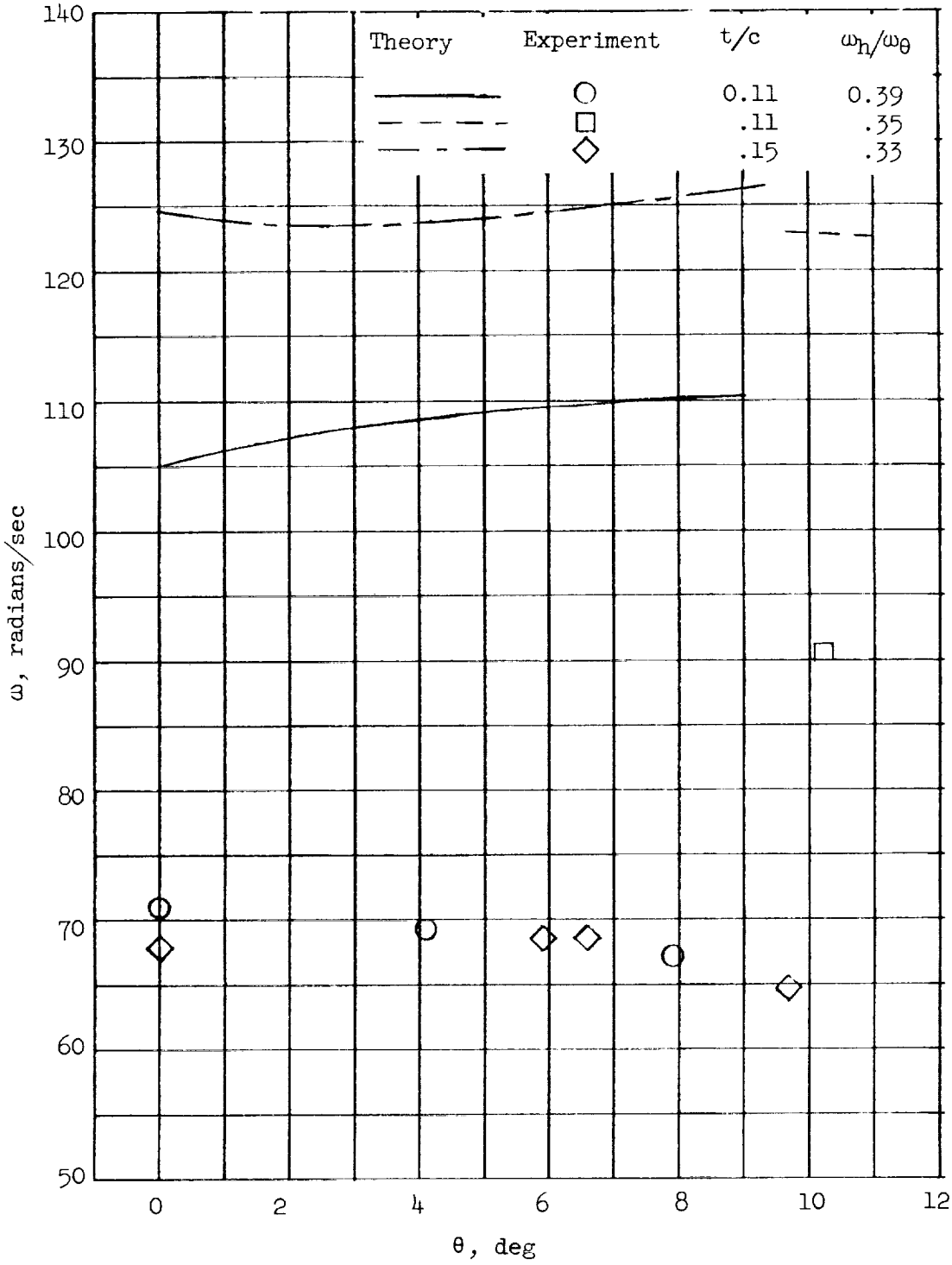

Figure 6.- Experimental and calculated flutter frequencies.